processes

MDPI

Article

Significance of Pressure Drop, Changing Molar Flow, and Formation of Steam in the Accurate Modeling of a Multi-Tubular Fischer–Tropsch Reactor with Cobalt as Catalyst

Andreas Jess * and Christoph Kern

Department of Chemical Engineering, Center of Energy Technology (ZET), University of Bayreuth, 95440 Bayreuth, Germany; christoph.kern@uni-bayreuth.de
* Correspondence: jess@uni-bayreuth.de

Abstract: A Fischer–Tropsch (FT) fixed-bed reactor was simulated with reactor models of different complexities to elucidate the impact of a pressure drop, a change in the total molar volume rate (induced by the reaction) along the tubes, and a change in the axial variation of the external radial heat transfer coefficient (external tube wall to cooling medium, here, boiling water) compared to disregarding these aspects. The reaction kinetics of CO conversion for cobalt as a catalyst were utilized, and the influence of inhibition of syngas (CO, H_2) conversion reaction rate by steam, inevitably formed during FT synthesis, was also investigated. The analysis of the behavior of the reactor (axial/radial temperature profiles, productivity regarding the hydrocarbons formed, and syngas conversion) clearly shows that, for accurate reactor modeling, the decline in the total molar flow from the reaction and the pressure drop should be considered; both effects change the gas velocity along the tubes and, thus, the residence time and syngas conversion compared to disregarding these aspects. Only in rare cases do both opposing effects cancel each other out. The inhibition of the reaction rate by steam should also be considered for cobalt as a catalyst if the final partial pressure of steam in the tubes exceeds about 5 bar. In contrast, the impact of an axially changing heat transfer coefficient is almost negligible compared to disregarding this effect.

Keywords: Fischer–Tropsch; pressure drop; gas recycle; inhibition by steam; fixed bed

Citation: Jess, A.; Kern, C. Significance of Pressure Drop, Changing Molar Flow, and Formation of Steam in the Accurate Modeling of a Multi-Tubular Fischer–Tropsch Reactor with Cobalt as Catalyst. *Processes* **2023**, *11*, 3281. https://doi.org/10.3390/pr11123281

Academic Editors: Tamás Varga and Blaž Likozar

Received: 20 September 2023
Revised: 15 November 2023
Accepted: 16 November 2023
Published: 23 November 2023

1. Introduction

An option for producing liquid fuels, such as diesel oil or jet fuel, which is not based on crude oil, is the Fischer–Tropsch synthesis (FTS). Currently, the synthesis gas for FTS (CO, H_2) is produced from coal or natural gas, e.g., in South Africa, Nigeria, Uzbekistan, and Qatar. In future, other, mainly non-fossil resources may also be considered for FTS: H_2 can be produced via water electrolysis using renewable energy, such as solar and wind. CO_2 is separated from the off-gases from power plants, from the off-gases from production of steel, cement, or industrial chemicals, or, in the future, also from air, as, for example, currently tested in the so-called Orca carbon-capture plant located near Reykjavik in Iceland.

Concentrated CO_2 (after conversion to CO) is then used as a carbon source for FT syngas, a mixture of H_2 and CO in a typical ratio of 2, e.g., via reverse water–gas shift ($CO_2 + H_2 \rightarrow CO + H_2O$) or, in future, potentially via the co-electrolysis of CO_2 and H_2O.

In two publications [1,2], we discussed the influence of the distribution of activity of a cobalt catalyst along the tubes on the operation of a cooled multi-tubular FT reactor with and without gas recycle and purge gas. However, the reactor model used so far to simulate the performance of a single tube—and, thus, in principle, of a technical FT reactor with up to 10,000 tubes by simply numbering up—still had drawbacks and simplifications as follows:

(1) The velocity of the gas u_s in the tubes was assumed as constant, which was an (over)simplification.

(2) The pressure drop, which affects the reaction rate and gas velocity (and, thus, residence time), was only calculated separately but not considered in the (as yet) isobaric reactor model.
(3) The decline in the total molar flow in the tubes via FT reaction—about 20% for a CO conversion of 50% (see Section 3.2)—was neglected, although this, accordingly, reduces gas velocity, increases residence time, and, through this—as explained descriptively—the conversion (to be precise, a lower molar flow raises the residual concentrations of CO and H_2 and, thus, the reaction rate and conversion compared to disregarding this effect).
(4) The heat transfer coefficient $\alpha_{w,ex}$ (external tube wall to boiling water) was assumed to be constant, but this depends on the pressure and temperature of the boiling water and—even more importantly—on the local value of the radial heat flux. Hence, $\alpha_{w,ex}$ varies along the tubes, and a maximum is located at the maximum of the axial temperature.
(5) The effective radial thermal conductivity λ_{rad} and, also, the heat transfer coefficient on the internal side of the wall $\alpha_{w,int}$ depend on u_s, but they were calculated simply based on the initial value of u_s, which was assumed to be constant and, hence, fixed in each model calculation. In reality, a change in gas velocity in the axial direction, induced by a pressure drop and/or a decrease in total molar flow from the reaction, changes both λ_{rad} and $\alpha_{w,in}$ in the axial direction in the tubes.
(6) The kinetic equations for the rate of CO conversion neglected any inhibiting influence of steam on the activity of the co-catalyst, which is not true for a high partial pressure of steam, particularly in the rear part of the tubes. Based on our experience, the influence is almost negligible for $p_{H2O} < 5$ bar, but it may be relevant if a higher value is reached [3].

We now implemented all these aspects in advanced reactor models and discussed step by step their individual and combined influence on the outcome, evaluated and compared via CO conversion and production of C_{2+}-hydrocarbons (HCs), in order to elucidate the significance of each factor in the accuracy of a model of an FT reactor and cooled fixed beds in general beyond FT. All these aspects have not been analyzed to date for a fixed-bed FT reactor.

The kinetics of FTS with Co as a catalyst, the methods of FT reactor modeling, and the data of technical FT reactors were presented in our own recent publication [1] and in the literature, e.g., [4–7].

2. Objectives and Methodology

2.1. Intrinsic and Effective Reaction Kinetics of Fischer–Tropsch Synthesis (FTS)

The main reaction of FTS is the formation of C_{2+}-hydrocarbons:

$$CO + 2H_2 \rightarrow (\text{-}CH_2\text{-}) + H_2O \; \Delta_R H_{CH2}{}^0{}_{298} = -152 \text{ kJ mol}^{-1} \quad (1)$$

The term (-CH_2-) represents a methylene group of a paraffinic hydrocarbon. In a (formal) kinetic description of the FTS, the formation of methane is often treated as a separate reaction:

$$CO + 3H_2 \rightarrow CH_4 + H_2O \; \Delta_R H_{CH4}{}^0{}_{298} = -206 \text{ kJ mol}^{-1} \quad (2)$$

The equations of the chemical rates of CO to CH_4 and C_{2+}-HCs in the absence of mass transfer limitations with cobalt as a catalyst (following an approach according to Langmuir–Hinshelwood) were already reported with all kinetic parameters [1]. Here, we only treat important aspects, such as the coefficient C_a (see below) and the impact of pore diffusion, in order to facilitate reading.

The intrinsic chemical rate of CO (without influence of mass transfer) is given by the formation rate of CH_4 and C_{2+}-HCs, as CO_2 formation by water–gas shift is negligible for a Co catalyst:

$$r_{m,\,CO} = -\frac{d\dot{n}_{CO}}{dm_{cat}} = C_a\,\left(r_{m,CO,\,CH_4} + r_{m,CO,\,C_{2+}}\right) \tag{3}$$

The intrinsic rates $r_{m,CO,CH4}$ and $r_{m,CO,C2+}$ were experimentally determined with a Pt-promoted (0.03 wt.% Pt to facilitate Co reduction) 10 wt.% Co/γ-Al_2O_3 catalyst [1]. The coefficient of activity C_a in Equation (3) considers the Co content and thus the purely chemical activity. C_a is set to one for 10% Co, and an increase/decline in C_a is considered to be realized by a rise or drop in the Co content. FT catalysts typically contain up to 30% Co ($C_a \approx 3$), a value mostly assumed in this study.

In this work, we have also extended the intrinsic rate equations by a term considering the inhibition by steam, which is relevant if a high concentration is reached in the rear part of the tubes. The re-evaluation of our experiments [3] yields the following (rough) approximation:

$$r_{m,\,CO,H_2O} = r_{m,\,CO}\left(1 - \frac{c_{H_2O}}{472\ \text{mol m}^{-3}}\right) \tag{4}$$

For example, a partial pressure of steam of 5 bar (120 mol/m^3 at 230 °C) leads to a decline in the intrinsic chemical reaction rate by 25%.

Equations (3) and (4) only reflect the intrinsic rate, but pore diffusion limitations decrease the effective rate compared to the intrinsic one for a particle size of several millimeters (here, d_p = 3 mm), relevant for FT fixed bed reactors to avoid an excessive pressure drop; the pores are filled with liquid hydrocarbons, and diffusion of CO and H_2 in liquid HCs is slow. As outlined in [1,2], the effectiveness factor η_{pore} and the related Thiele modulus ϕ are:

$$\eta_{pore} = \frac{r_{m,CO,eff}}{r_{m,CO}} = \frac{\tanh\phi}{\phi} \approx \frac{1}{\phi}\ \text{for}\ \phi > 2 \tag{5}$$

$$\phi = \left\{\frac{d_p}{6}\sqrt{\frac{\rho_{cat}}{D_{eff,CO,liq}\ \frac{R\,T}{H_{CO}}}}\right\}\sqrt{\frac{r_{m,CO}}{c_{CO}}} = C_\phi\sqrt{C_a\frac{\left(r_{m,CO,\,CH_4} + r_{m,CO,\,C_{2+}}\right)}{c_{CO}}} \tag{6}$$

For the particle diameter of 3 mm, as assumed here, C_ϕ is 300 $kg^{0.5}\ s^{0.5}\ m^{-1.5}$; see previous publication [1]. The effective rate of CO conversion is then given based on Equations (3)–(6) by:

$$r_{m,CO,eff} = \eta_{pore}\ r_{m,CO} \tag{7}$$

For a diameter of the particles of 3 mm, η_{pore} is lower than 1 above 180 °C and reaches a value of around 0.2 for 240 °C (C_a = 3) [1,2]. The mean molar H_2-to-CO ratio within the particles is then higher compared to the free gas phase with a value of about two. The unwanted formation of CH_4 then rises and lower HCs are formed, as the diffusion coefficient of H_2 in liquid HCs is by a factor of two higher compared to CO. This impact is strong above 240 °C and the CH_4 selectivity (S_{CH4}) then exceeds 20% by weight compared to 10% in the absence of diffusion limitations [1]. In this study, we therefore limited the temperature to 240 °C and assumed that S_{CH4} is constant at 20%, i.e., 80% of CO is converted to C_{2+}-HCs. We fixed the H_2-to-CO ratio in the fresh syngas to 2.2, and the H_2 conversion then equals that of CO, which simplifies all mass balances [2].

It should be mentioned that a limitation of the effective reaction rate by external mass transfer does not play a role in Fischer–Tropsch synthesis as FTS is a rather slow reaction; the strong influence of internal mass transfer only occurs if the pores are filled with liquid hydrocarbons. In case of gas-filled pores, i.e., in the initial phase of FTS with a fresh catalyst, even internal diffusion limitations are negligible.

If inhibition of the effective rate by steam is considered, Equations (5) and (6) with $r_{m,CO,H2O}$ instead of $r_{m,CO}$ are valid. For a strong limitation by pore diffusion (ϕ > 2:

$r_{m,CO,H2O,eff} = \eta_{pore}\ r_{m,CO,H2O} \sim r_{m,CO,H2O}{}^{0.5}$), as typical for fixed-bed FT synthesis, inhibition of the effective rate by steam is weaker than that of the intrinsic rate, e.g., for a partial pressure of steam of 5 bar, the effective rate drops only by 13% and not by 25%, as stated before for the decline of the intrinsic rate.

2.2. Models (Examined in This Work) of a Multi-Tubular FT Reactor Cooled by Boiling Water

The model to simulate a single tube of a multi-tubular fixed-bed reactor is a pseudo-homogenous two-dimensional model already presented [1,2].

The mass and the heat balance in a differential axial tube section are given by the following Equations (8) and (9):

$$\frac{d(c_i\ u_s)}{dz} = \left(\nu_{i,R1}\ r_{m,CO,R1,eff} + \nu_{i,R2}\ r_{m,CO,R2,eff}\right)\ \rho_{bed} \tag{8}$$

$$c_p\ \rho_g \frac{d(T\ u_s)}{dz} = \lambda_{rad} \frac{1}{r} \frac{dT}{dr} + \lambda_{rad} \frac{d^2T}{dr^2} + \left(\ r_{m,CO,R1,\ eff}(-\Delta_R H_{R1}) + r_{m,CO,R2,eff}(-\Delta_R H_{R2})\right)\ \rho_{bed} \tag{9}$$

Radial temperature gradients in the bed are taken into account to achieve a reliable calculation of the operation of the FT reactor (temperature profiles in the axial and radial direction, CO conversion, and thermal stability). Each reactor tube has an inner diameter $d_{t,int}$ of 3 cm. The heat produced by FTS is radially transferred through the pseudo-homogenous phase consisting of catalyst and gas from the fixed bed to the inner tube wall. The radial heat flux within the bed is governed by the radial effective thermal conductivity λ_{rad} and the internal heat transfer coefficient $\alpha_{w,int}$, taking into account the thermal resistance very near the internal side of the wall resulting from the high porosity of the bed at the wall. Finally, heat transfer by conduction in the wall, which only negligibly contributes to the total thermal resistance, and the heat transfer from the external side of the tubes to the boiling water are also considered in the reactor model.

Both the axial dispersion of mass and of heat were deliberately neglected in the reactor model as they are only relevant if very steep axial gradients of concentration or temperature over a length of a few particles are present. This may be different for radial dispersion of mass if the radial difference in temperature in the fixed bed becomes large, e.g., near or during temperature runaway. We then may have a difference of 50 K or more over a length of about 5 particles (radius of tube: 15 mm; particle diameter 3 mm) and not only about 10 K as during "normal" operation (see Figure S14 in the Supporting Information), and the reaction rate near the (cooler) wall is then much lower compared to the center region of the tubes. In the former case, the syngas conversion is relatively low (high concentration) near the wall and high (low concentration) in the center region. Hence, radial dispersion then may lead to a radial "mixing", i.e., to an adjustment of radial concentration gradients by "dispersive" supply of CO and H_2 from the near-wall region to the tube center. This effect may then, for example, decrease the ignition temperature to a certain extent compared to the case of no radial dispersion of mass. This aspect is, here, not further considered but will be analyzed in future work in more detail.

Table 1 shows parameter values utilized to model an FT reactor with gas recycle (unconverted CO and H_2, and CH_4), a purge gas stream, and an assumed total CO conversion of 95%. The values are given for a superficial gas velocity of 1 m/s.

It should be mentioned that the results of modeling of an FT reactor depend on the specific catalyst used, e.g., on the main active metal, here, Co and not Fe, as also industrially used for FTS. Here, we concentrate on cobalt as a catalyst and used our own experimental results of the kinetics.

Table 1. Parameter values used to model the FT reactor with gas recycle and a total CO conversion of 95% (details on heat transfer in Supporting Information).

Constant Parameters (230 °C, 30 bar) Not Varied during Modeling		**Value**
Length of reactor (single tube) L_t		12 m [a]
Internal tube diameter $d_{t,int}$		3 cm
Thickness of tube wall s_{wall}		0.3 cm
Content of CO (in fresh syngas) $y_{CO,fresh,SG}$		0.3125
Content of H_2 (in fresh syngas) $y_{H2,fresh,SG} = 1 - y_{CO,fresh,SG}$		0.6875
Total pressure p_{total}		30 bar
Diameter of spherical catalyst particles d_p		3 mm
Bulk density of bed/catalyst ρ_{bed}		960 kg m^{-3}
Porosity of fixed bed ε_{bed}		0.4
Heat capacity of gas mixture c_p		29 J mol^{-1} K^{-1}
Thermal conductivity of gas mixture λ_g		0.016 W m^{-1} K^{-1}
Kinematic viscosity of gas mixture ν_g		2.3×10^{-6} m^2 s^{-1}
Thermal conductivity of wall material (steel) λ_{wall}		15 W m^{-1} K^{-1}
Parameters varied during modeling	**Comment**	**Typical value**
Content of CO (inlet of reactor) $y_{CO,reactor,in}$	depends on X_{CO} and corresponding recycle ratio R	0.19 [b]
Content of H_2 (inlet of reactor) $y_{H2,reactor,in}$		0.42 [b]
Content of CH_4 (inlet of reactor) $y_{CH4,reactor,in}$ [c]		0.39 [a]
Pressure drop Δp_{bed}	depends on u_s	5.6 bar [b]
Initial superficial gas velocity $u_{s,z=0}$ (230 °C, 30 bar)	varied	1 m s^{-1}
Heat transfer coefficient (wall to boiling water) $\alpha_{w,ex}$	depends on u_s [d]	1850 W m^{-2} K^{-1}
Effective radial thermal conductivity λ_{rad}		8.4 W m^{-1} K^{-1}
Heat transfer coefficient (bed to internal tube wall) $\alpha_{w,int}$		1540 W m^{-2} K^{-1}

[a] The length of the tubes of industrial multi-tubular FT reactors are typically in a range of 12 to 20 m [6,7]. [b] Values according to model M4 for $u_{s,z=0}$ = 1 m/s and C_a = 3. [c] The recycle and purge gas is considered to contain only unconverted CO and H_2 and CH_4. It is assumed that H_2O and all C_{2+}-HCs are separated as liquids downstream of the reactor (see [2]). [d] λ_{rad} and $\alpha_{w,int}$ depend on u_s, which changes along the tubes due to pressure drop and decreasing total molar flow rate. The values listed are initial values at the tube inlet for $u_{s,z=0}$ = 1 m/s. $\alpha_{w,ex}$ mainly depends on the local radial heat flux. The listed value is the one at z = 1.9 m, where the maximum axial temperature of 240 °C is just reached for u_s = 1 m/s and C_a = 3. $\alpha_{w,ex}$ also includes heat conduction through the wall; see Equation (S18) in the Supporting Information.

As mentioned in the introduction, we have now modified and improved the reactor model by considering the pressure drop as well as the decline in the total molar flow, which both influence the gas velocity and residence time. An axially changing gas velocity also influences the radial conductivity λ_{rad} and the internal heat transfer coefficient $\alpha_{w,int}$. All heat transfer parameters were calculated by literature correlations [8–14]; see Supporting Information.

The influence of pressure of the boiling water and of the radial heat flux was also taken into account for an accurate determination of the local value of the external heat transfer coefficient $\alpha_{w,ex}$.

Finally, we also analyzed the impact of the inhibition of the CO reaction rate by steam on the outcome of a model of a cooled multi-tubular FT reactor.

Table 2 introduces the used models and the respective parameters considered or deliberately neglected to clearly elucidate step by step the influence of all these aspects

on the outcome of each model, i.e., the FT reactor performance, mainly "measured" by $X_{CO,per\ pass}$ and production rate of C_{2+}-HCs.

Table 2. Reactor models used here for a multi-tubular fixed-bed FT reactor.

Label of Model	Parameter Considered (+)or Neglected (−)			Comment
	$\Delta\dot{n}_{total}$	p_{bed}	Impact of H_2O	
M0	−	−	−	"Simple" model used in previous publications [1,2] (constant u_s, p_{total}, $\dot{n}_{total}$, and $\alpha_{w,ex}$ (1 kW m^{-2} K^{-1})
M1	−	−	−	As model M0, but accurate calculation of $\alpha_{w,ex}$ (for details see Section 3.1)
$M2_n$	+	−	−	Used to show only effect of $\Delta\dot{n}_{total}$ (and of corresponding axial drop of u_s), i.e., neglecting p_{bed}
$M2_p$	−	+	−	Used to show only effect of p_{bed} (and of corresponding axial rise of u_s), i.e., neglecting change of $\dot{n}_{total}$
M3	+	+	−	Accurate model, if inhibition by steam is negligible
M4	+	+	+	As M3, but also considering inhibition by steam

Details on the general performance of an FT reactor including a gas recycle and a purge gas stream were already outlined in our very recent publication [2]. Here, we have always assumed a total syngas conversion (CO, H_2) of 95%, realized by a respective recycle ratio R and a purge gas stream, which is needed as an outlet for all unwanted methane produced as a by-product.

The gas velocity and the syngas composition at the reactor entrance, depending on the total and per pass conversion of CO ($X_{CO,total}$, $X_{CO,per\ pass}$), were varied, but the geometry of the tubes (internal diameter 3 cm, length 12 m), the initial total pressure (30 bar), and T_{max} (240 °C) were fixed. The critical cooling (ignition) temperature T_{ig}, where thermal runaway occurs, was determined in every modeling case. For a safe operation, the maximum of the cooling temperature was fixed to be 5 K below the temperature of ignition (T_{ig}).

The equations of the mass and heat balances (listed in Supporting Information) were solved by the program Presto, a solver of differential equations (CiT GmbH, Rastede, Germany).

During reactor modeling, the catalytic activity (coefficient C_a) was mostly regarded as constant. Only in two cases an axial activity distribution was considered, a two-zone fixed-bed and a graded distribution with $C_{a,initial}$ until T_{max} of 240 °C was reached followed by a continuous increase in C_a to keep the temperature at 240 °C, as presented in the Supporting Information (Table S1).

In this work, we use a value for C_a of three (ideally 30% Co) as the appropriate value for a superficial gas velocity around 1 m/s (and C_a = 2 for 0.5 m/s) to guarantee a safe operation of the reactor; details are given in a former publication [2].

The initial superficial gas velocity at the entrance of the tubes ($u_{s,z=0}$) was varied in a broad regime from 0.25 m/s to 1.6 m/s, as this has a strong influence on Δp_{bed}, $X_{CO,per\ pass}$, production rate of C_{2+}-HCs, heat transfer parameters, and on the change in u_s in axial direction:

- If Δp_{bed} is low (low $u_{s,z=0}$), u_s drops along the tubes and, in return, the residence time (compared to constant u_s) increases by the then dominating effect of the drop in the total molar flow rate. This, in return, has an influence on the local values (axial

direction) of $\alpha_{w,int}$ and λ_{rad}. In total, $X_{CO,per\ pass}$ is then higher compared to a model (as M0 or M1, Table 2) simplified assuming a constant u_s.

- If Δp_{bed} is high (high $u_{s,z=0}$), this yields an increase in u_s in axial direction (decrease in residence time compared to constant u_s), as the drop in u_s by the decreasing total molar flow rate is then overcompensated; this again has an impact on the local values of $\alpha_{w,ex}$ and λ_{rad}, and, in total, $X_{CO,per\ pass}$ is then lower compared to a model assuming constant u_s.
- For a "medium-sized" Δp_{bed} (medium-sized $u_{s,z=0}$), we may obtain an almost constant gas velocity along the tubes, i.e., the opposite influence of Δp_{bed} and drop in total molar flow on u_s cancel each other out. In this rare case, a model with or without considering both aspects coincidentally yields similar results with regard to $X_{CO,per\ pass}$ or production rate of C_{2+}-HCs.

3. Results of Simulation of a Single Tube of a Cooled Multi-Tubular FT Reactor

3.1. Influence of External Heat Transfer Coefficient $\alpha_{w,ex}$ on Reactor Modeling

In contrast to the "simple" model M0, used in our previous publications [1,2], all other models consider the influence of the pressure of the boiling water and of the local radial heat flux, which changes in axial direction (Figure 1), on the external heat transfer coefficient $\alpha_{w,ex}$ based on literature correlations (Supporting Information) [12–14]. This effect was neglected in model M0, where an estimated constant value of $\alpha_{w,ex}$ (1 kW m^{-2} K^{-1}) was used (Figure 1). The heat transfer parameters λ_{rad} and $\alpha_{w,int}$, both depending via Re_p on the gas velocity, Figure S1, were calculated by literature correlations [4–8] (Supporting Information). For M0 and M1, both assuming constant u_s and p_{total}, λ_{rad} and $\alpha_{w,int}$ are constant (Figures 1 and 2).

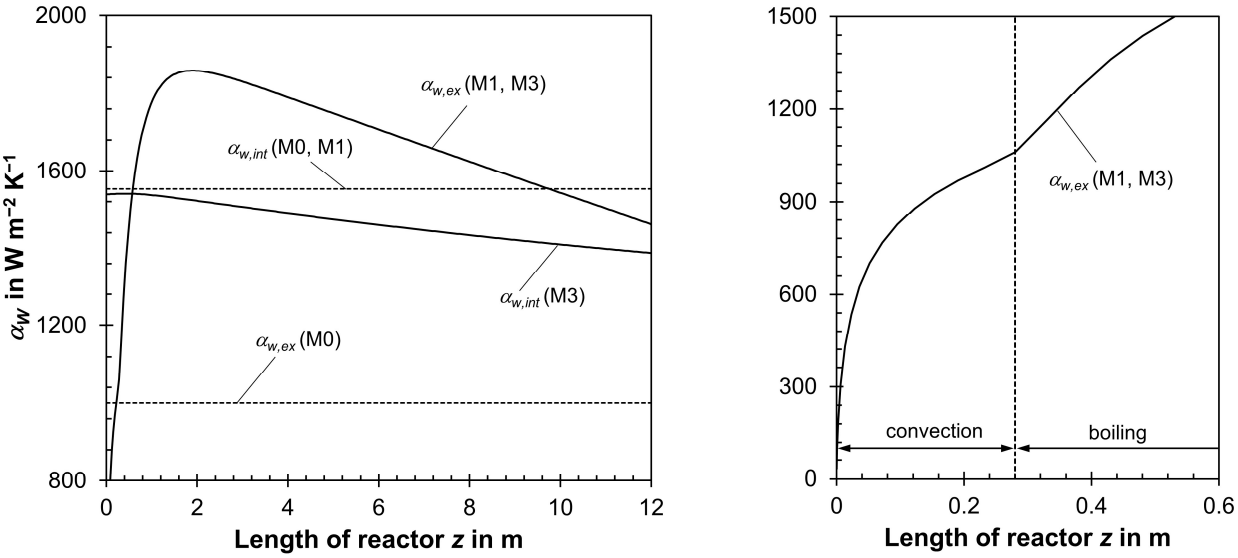

Figure 1. Heat transfer coefficient from fixed bed to inner tube wall at $r = r_t$ ($\alpha_{w,int}$) and heat transfer coefficient from external tube wall to boiling water ($\alpha_{w,ex}$) of a multi-tubular FT reactor according to the models M0, M1, and M3. (**left**) shows the profiles of $\alpha_{w,int}$ and $\alpha_{w,ex}$ in the whole tube ($0 < z < 12$ m). Conditions: $C_a = 3$, $u_{s,z=0} = 1$ m/s, $p_{total} = 30$ bar, $d_p = 3$ mm, $d_{t,int} = 3$ cm, $L_t = 12$ m, $H_2/CO = 2.2$. Axial profile of Re_p is shown in Figure S2. Details of $\alpha_{w,ex}$ (**right**) in the entrance region ($z < 0.6$ m) show that convection boiling dominates in the front section ($z < 0.24$ m) with a still rather low heat flux; for $z > 0.24$ m, we then have nucleate boiling and a strong rise in $\alpha_{w,ex}$. Also note that $\alpha_{w,ex}$ formally also includes heat conduction through the tube wall, see Equation (S18) and Figure S3, although this contribution is rather small.

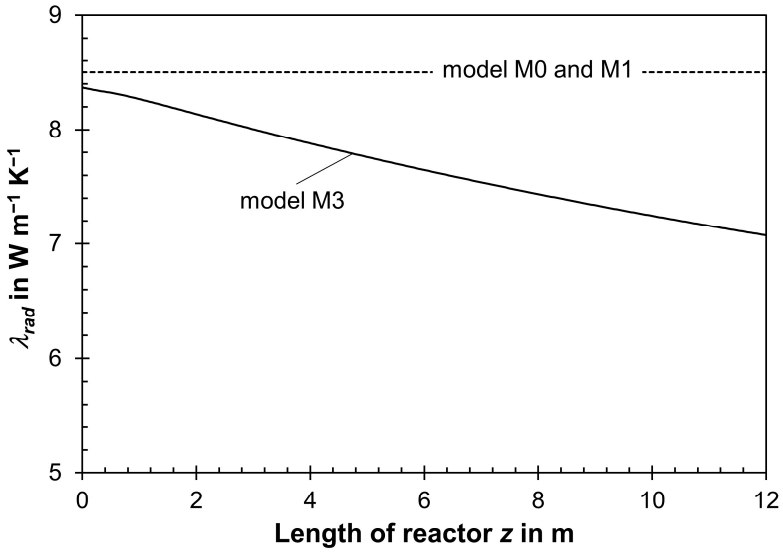

Figure 2. Radial thermal conductivity in the fixed bed (λ_{rad}) of a multi-tubular FT reactor according to model M0, M1, and M3 (C_a = 3, $u_{s,z=0}$ = 1 m/s, p_{total} = 30 bar, d_p = 3 mm, $d_{t,int}$ = 3 cm, L_t = 12 m, molar H_2-to-CO ratio = 2.2). For axial profile of Re_p, see Figure S2.

For model M1 (and also M2 to M4), the external heat transfer coefficient $\alpha_{w,ex}$ passes a maximum at z = 2 m (Figure 1), corresponding to the location of the maximum temperature (Figure 3) and the highest radial heat flux. The comparison of M0 and M1, which only differ in value and calculation of $\alpha_{w,ex}$ (Figure 1), shows that the model data are similar, e.g., $X_{CO,per\ pass}$ is 44.3% (model M0) and 45.5% (M1), Table 3. Nevertheless, the more accurate calculation of $\alpha_{w,ex}$, implemented in all models except model M0, should be preferred and was, here thereafter, utilized.

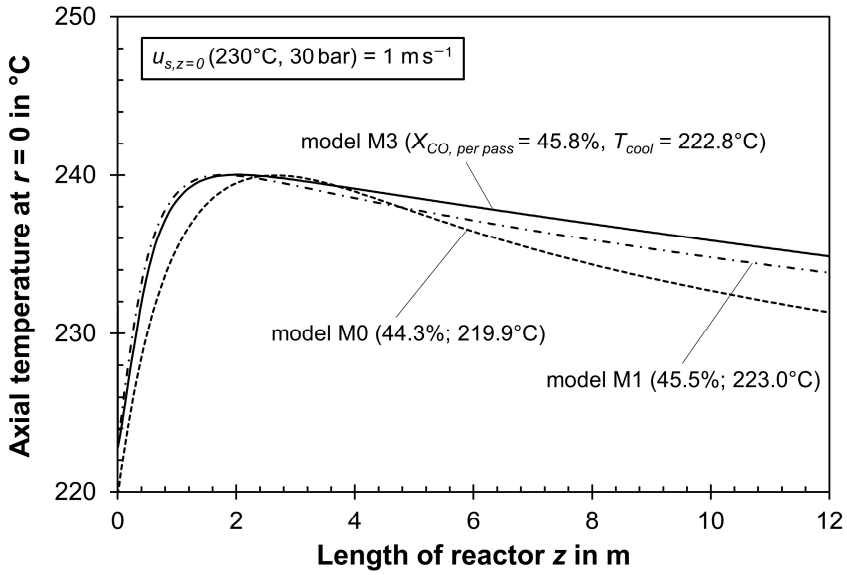

Figure 3. Temperature profiles in axial direction at r = 0 (center of tube) for model M3 (considering Δp_{bed} and change in total molar flow rate by reaction). The results of model M0 and M1 (both assuming constant u_s) are also shown (C_a = 3; $u_{s,z=0}$ (230 °C, 30 bar) = 1 m/s; other conditions in Table 4). Profiles of the reaction rate are shown in Figure S4.

Table 3. Data of multi-tubular FT reactor according to the models M0 (with constant value of $\alpha_{w,ex}$) and M1 (improved calculation of $\alpha_{w,ex}$; see text and Figure 1) for constant u_s of 1 m/s (230 °C, 30 bar) and C_a = 3. Conditions: $X_{CO,total}$ = 95%; S_{CH4} = 20%; molar H_2-to-CO ratio = 2.2; T_{max} = 240 °C; 1825 mol/h syngas per tube at reactor inlet.

T_{cool} in °C	$X_{CO,per\ pass}$ in %	$y_{CH4,reactor,in}$ in %	R	Prod. of C_{2+}-HCs per Tube in kg_C per h	Reactor Model and Parameter Considered (+) or Neglected (−)			
					Model	$\alpha_{w,ex} = f(z)$	$\Delta\dot{n}_{total}$	p_{bed}
219.9	44.3 [a]	38.7	2.50	1.48	M0	−	−	−
223.0	45.5	38.1	2.38	1.54	M1	+ (see Figure 1)	−	−

[a] Throughout this work, we have chosen a precision for the CO conversion (and other parameters) of three significant digits (e.g., here, 44.3%). A higher precision is not justified (also with regard to the insufficient knowledge of the "exact" values of kinetic, heat transfer parameters, etc.). In addition: for a constant maximum axial temperature (here, 240 °C), the value calculated by the model is not exactly 240.00 °C but typically in a range of 239.98 and 240.02 °C to limit the time needed for the variation in the cooling temperature to reach the target value of 240.00 °C. Hence, the normalized rate and thus the conversion are then in a range of 0.9993 and 1.007 of the "true" value of 1.000.

Table 4. Data of multi-tubular fixed-bed FT reactor according to the reactor models M1, $M2_n$, $M2_p$, and M3 for $u_{s,z=0}$ = 1 m/s (230 °C, 30 bar) and C_a = 3. Conditions: $X_{CO,total}$ = 95%, S_{CH4} = 20%, molar H_2-to-CO ratio = 2.2, T_{max} = 240 °C, 1825 mol/h syngas per tube at reactor inlet. Further details are shown in the Figure S4.

T_{cool} in °C	$X_{CO,per\ pass}$ in %	$y_{CH4,reactor,in}$ in %	R	Prod. of C_{2+}-HCs per Tube in kg_C per h	Reactor Model and Parameters Considered (+) or Neglected (−)			
					Model	$\Delta\dot{n}_{total}$	p_{bed}	Impact of H_2O
223.0	45.5	38.1	2.38	1.54	M1	−	−	−
222.5	49.1	36.2	2.05	1.72	M2n	+	−	−
223.5	42.6	39.6	2.69	1.41	M2p	−	+	−
222.8	45.8	37.9	2.35	1.56	M3	+	+	−

3.2. Influence of Pressure Drop and Change in Total Molar Gas Flow on Reactor Modeling

Table 4 and Figures 3–5 show the results of the reactor simulation by models M1, $M2_p$, $M2_n$, and M3 for an initial superficial gas velocity $u_{s,z=0}$ of 1 m/s (230 °C, 30 bar).

According to the "correct" model 3 (within the four models compared here), which considers Δp_{bed} as well as $\Delta\dot{n}_{total}$, the gas velocity u_s is almost constant, as discussed below in detail. Nevertheless, both the effective radial thermal conductivity λ_{rad} (Figure 2) and the internal heat transfer coefficient $\alpha_{w,int}$ (Figure 1) decrease to a certain extent along the tubes by the decline in Re_p (=$u_s\ d_p/\nu_g$), Figure S2, as the gas viscosity (ν_g) rises with decreasing pressure (ν_g~$1/p_{total}$). But this effect only leads to minor differences in the axial profiles of temperature (center of tube) and reaction rate for models M1 and M3 (Figure 3 and Figure S4), and the CO conversion per pass and production rate of C_{2+}-HCs are very similar, Table 4 (first and fourth row).

If only the decline in $\dot{n}_{total}$ (and not Δp_{bed}) is implemented in the model (as for $M2_n$), the conversion is much larger (49.1%) as for the models M1 (45.5%) and M3 (45.8%), see Table 4. For model $M2_p$, considering only Δp_{bed}, this is reversed and $X_{CO,per\ pass}$ is only 42.6%. Hence, an accurate model should consider both Δp_{bed} and $\Delta\dot{n}_{total}$ (as M3) and not only one of these two aspects ($M2_p$ and $M2_n$), as this even leads to less reliable data than neglecting both aspects (M1).

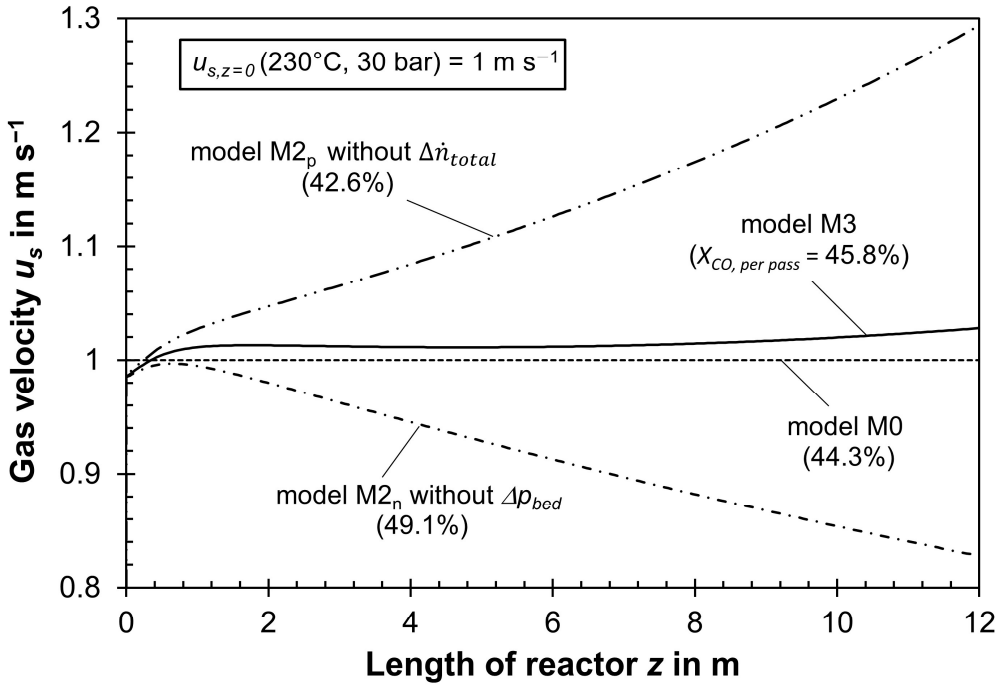

Figure 4. Axial profiles of gas velocity u_s for model M3 (considering Δp_{bed} and change in total molar flow rate). Results of model $M2_n$ and $M2_p$ (considering only change in molar flow rate and not of Δp_{bed} or vice versa) and M0 (assuming constant u_s and constant $\alpha_{w,ex}$) are also shown (C_a = 3; $u_{s,z=0}$ (230 °C, 30 bar) = 1 m/s; other data in Table 4).

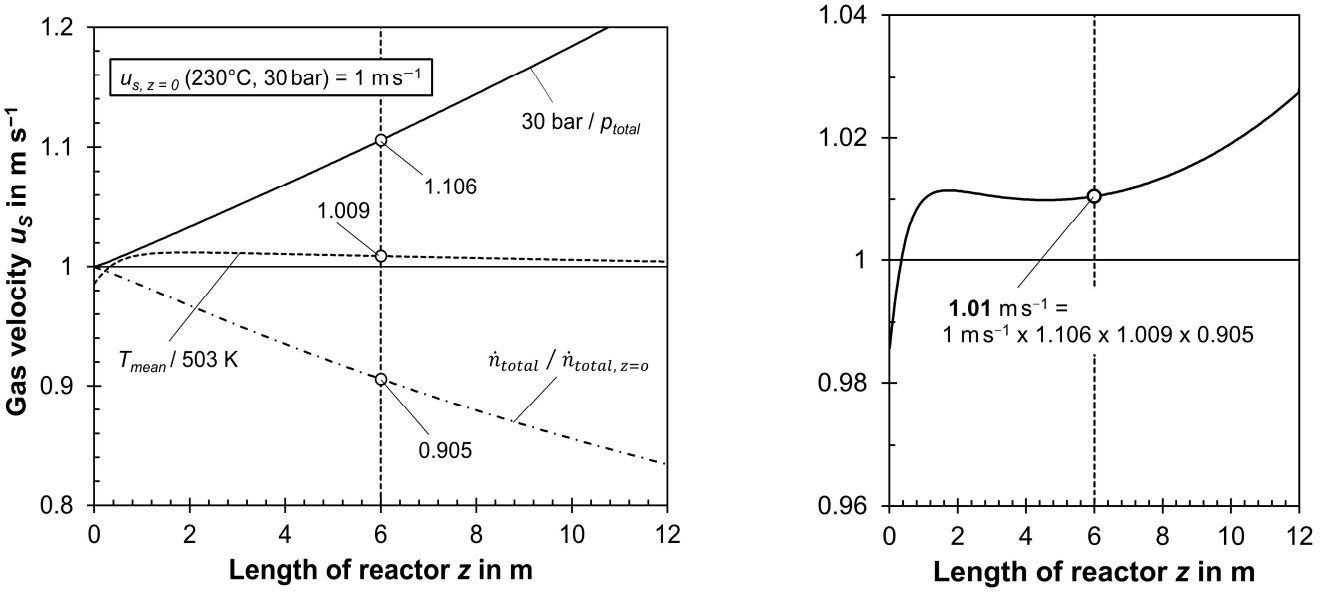

Figure 5. Individual (**left**) and combined contributions (**right**) to change in gas velocity u_s (1 m/s at reactor entrance for 230 °C and 30 bar) according to model M3: (1) change in p_{total} by Δp_{bed}, i.e., u_s~30 bar/p_{total} = 30 bar/(30 bar − Δp_{bed}); (2) change in T, i.e., u_s~T/503 K; (3) change in total molar flow rate by reaction, i.e., u_s~$\dot{n}_{total}/\dot{n}_{total,\ z=o}$. Conditions: C_a = 3; $u_{s,z=0}$ (230 °C, 30 bar) = 1 m/s; other conditions in Table 4.

Figure 5 shows the individual (left) and combined influence (right) of temperature, Δp_{bed}, and drop in total molar flow rate on the gas velocity u_s in more detail for model M3. For an initial value of $u_{s,z=0}$ of 1 m/s, the influence of $\Delta\dot{n}_{total}$ and Δp_{bed} on u_s cancel each other out; the impact of temperature on u_s is negligible, as the (mean) value only varies in a range of 223 to 240 °C.

Table 5 and the Figures 6 and 7 show the results of models M1, $M2_n$, $M2_p$, and M3 but, now, for a relatively low initial gas velocity u_s of 0.5 m/s (230 °C, 30 bar). For this rather low gas velocity, Δp_{bed} is almost negligible, only 1.2 bar compared to 5.6 bar for $u_{s,z=0}$ = 1 m/s, and the gas velocity substantially decreases along the tubes by up to about 25% (Figure 7) if models M3 and $M2_n$ are used, both considering the drop of the molar flow rate by the FT reaction. In return, the CO conversion per pass (62.8% and 63.4%, respectively) is then higher compared to the "simple" model 1 (56.9%; Table 5), which assumes (too simplifying) a constant gas velocity. Hence, for a low gas velocity, a model not implementing $\Delta \dot{n}_{total}$ should not be used or only for rough estimations. Model $M2_p$, only considering Δp_{bed} compared to M1, shows that the implementation of (low) Δp_{bed} only is of minor importance (Table 5).

Table 5. Data of a multi-tubular FT reactor according to models 1, 2_n, 2_p, and 3 for $u_{s,z=0}$ = 0.5 m/s (230 °C, 30 bar) and C_a = 2. Conditions: $X_{CO,total}$ = 95%; S_{CH4} = 20%; molar H_2-to-CO ratio = 2.2; T_{max} = 240 °C; 912.5 mol/h syngas per tube at reactor inlet.

T_{cool} in °C	$X_{CO,per\ pass}$ in %	$y_{CH4,reactor,in}$ in %	R	Prod. of C_{2+}-HCs per Tube in kg_C per h	Reactor Model and Parameters Considered (+) or Neglected (−)			
					Model	$\Delta \dot{n}_{total}$	p_{bed}	Impact of H_2O
218.0	57.7	31.4	1.41	1.08	M1	−	−	−
216.6	63.4	27.9	1.09	1.25	$M2_n$	+	−	−
218.2	57.1	31.7	1.45	1.07	$M2_p$	−	+	
216.9	62.8	28.3	1.12	1.23	M3	+	+	−

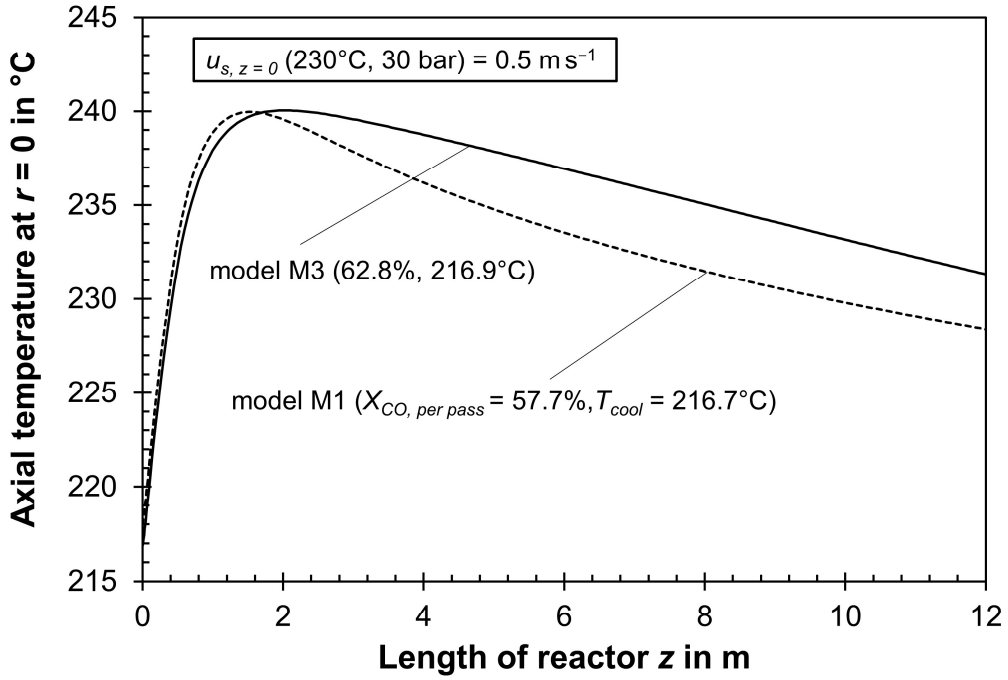

Figure 6. Profiles of axial temperature at r = 0 (center of tube) in a tube of a cooled multi-tubular FT reactor for model M3 (considering Δp_{bed} and change in total molar flow rate by reaction). For comparison, model M1 (without Δp_{bed} and assuming constant u_s) is also shown. Conditions: C_a = 2; $u_{s,z=0}$ (230 °C, 30 bar) = 0.5 m/s; other conditions are listed in Table 4. The corresponding profiles of the reaction rate are depicted in Figure S5.

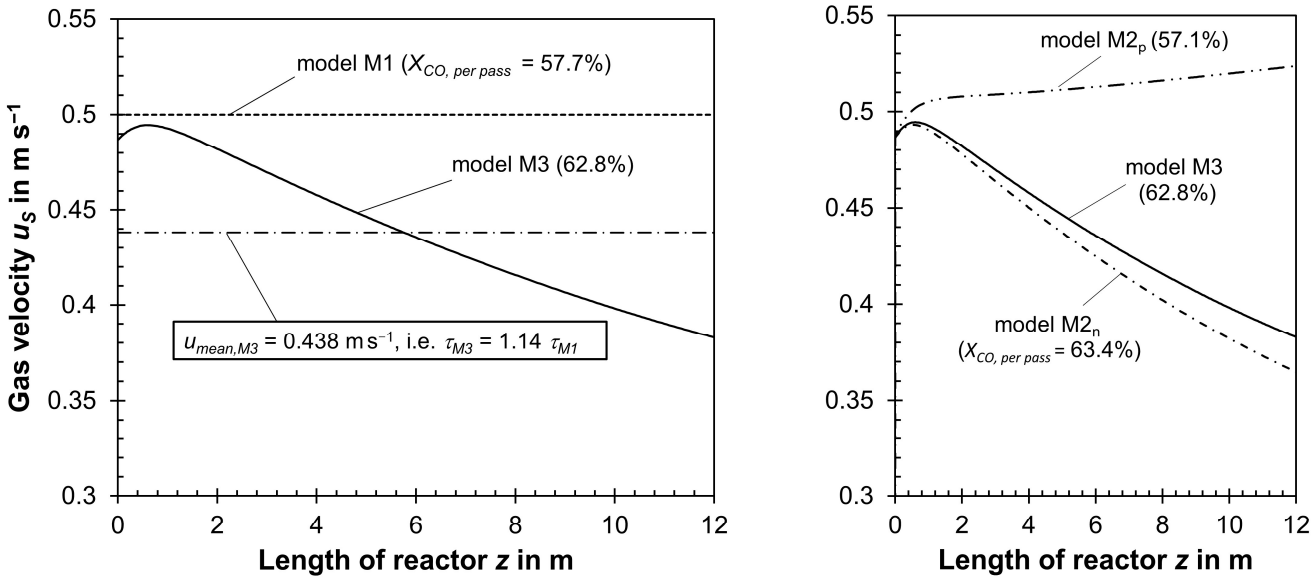

Figure 7. Profiles of gas velocity u_s in a single tube for model M3 (considering Δp_{bed} and change in molar flow rate). For comparison, results of model M1 (**left**; assuming constant u_s), model $M2_n$, and $M2_p$ (**right**; considering only change of total molar flow rate or of total pressure, respectively) are also shown. Conditions: C_a = 2; $u_{s,z=0}$ (230 °C, 30 bar) = 0.5 m/s; other conditions in Table 5. Horizontal lines (left) represent mean values.

Two additional figures are given in the Supporting Information: Figure S4 depicts axial profiles of the effective rate at r = 0 (center of tube) for model 1 and 3 for $u_{s,z=0}$ = 1 m/s and Figure S5 for 0.5 m/s. Again, note that effectiveness factor η_{pore} (center of tube, i.e., at r = 0) is, here, always only around 0.2.

3.3. Influence of Inhibition of Steam on the Performance of an FT Reactor

Table 6 compares the influence of considering the inhibition of the reaction rate of CO conversion by steam on the reactor modeling for initial gas velocities (at 230 °C and 30 bar) of 0.5 and 1 m/s. Now, only the "advanced", most accurate models M3 and M4 are considered, i.e., both $\Delta \dot{n}_{total}$ and Δp_{bed} are implemented but either without (M3) or with (M4) steam inhibition.

Table 6. Data for model M3 (no inhibition by steam) and model M4 (inhibition). Conditions: $X_{CO,total}$ = 95%; S_{CH4} = 20%; molar H_2-to-CO ratio = 2.2; T_{max} = 240 °C; 1825 or 912 mol/h syngas per tube at inlet for $u_{s,z=0}$ of 1 or 0.5 m/s (details in Figures S6 and S7).

T_{cool} in °C	$X_{CO,per\ pass}$ in %	$y_{CH4,reactor,in}$ in %	R	Production of C_{2+}-HCs per Tube in kg_C per h	Reactor Model and Parameters Considered (+) or Neglected (−)			
					Model	$\Delta \dot{n}_{total}$	p_{bed}	Impact of H_2O
$u_{s,z=0}$ = 1 m/s (230 °C, 30 bar); C_a = 3								
222.8	45.8	37.9	2.35	1.56	M3	+	+	−
223.1	44.4 [a]	38.7	2.49	1.49	M4	+	+	+
$u_{s,z=0}$ = 0.5 m/s (230 °C, 30 bar); C_a = 2								
216.9	62.8	28.3	1.12	1.23	M3	+	+	−
217.6	59.0 [b]	30.6	1.34	1.12	M4	+	+	+

[a] p_{H2O} at the end of the tubes (z = 12 m) is 2.5 bar, i.e., the intrinsic rate (Equation (4) is about 13% lower compared to no inhibition by steam; the effective rate then declines by only 7%, Equations (5) and (6). [b] p_{H2O} at z = 12 m is 4.8 bar, i.e., the intrinsic rate is 25% lower compared to no inhibition; the effective rate then declines by 13%.

For model M4, which correctly considers inhibition by steam, the CO conversion per pass is, as expected, in general, lower at 44.4% compared to 45.8% for M3 for $u_{s,z=0}$ of 1 m/s, which is still a small deviation, as p_{H2O} only reaches 2.5 bar at the end of tubes. For a lower initial gas velocity of 0.5 m/s, the deviation of conversion is already quite pronounced at 59% for model M4 compared to 62.8% for M3. Now, a rather high value of p_{H2O} of 4.8 bar is reached at the reactor outlet. In conclusion, an accurate FT reactor model should include inhibition by steam if the conversion per pass is above 50% and if p_{H2O} finally approaches 5 bar, respectively.

In order to spotlight the even more pronounced influence of inhibition by steam on the reactor modeling for X_{CO} >> 50%, we then used "extreme" parameters, a low value for $u_{s,z=0}$ of 0.5 m/s, a high value of C_a of 4, and a syngas consisting only of CO and H_2. In addition, the reactor was (contrary to industrial reality) considered as isothermal ($\Delta_R H_i$ was then just zeroized in the model), and a high temperature of 240 °C was chosen to reach a high CO conversion and, thus, a high partial pressure of steam in the rear part of the tubes (Table 7, see also Figures S6 and S7 in the Supporting Information). Now, the CO conversion is 81% and 92% with and without inhibition. Thus, model M4 considering inhibition by steam is then clearly needed for a reliable simulation.

Table 7. Data of isothermal FT reactor (240 °C) for model M4 (considering Δp_{bed}, change in total molar flow, and inhibition by steam) and for M3 (as M4 but without influence of steam) for $u_{s,z=0}$ of 0.5 m/s and C_a of 4 (syngas with 31.3% CO and 68.7% H_2).

CO Conversion X_{CO} at Axial Position z			p_{H2O} (y_{H2O}) at z = 12 m	u_s at z = 12 m	**Reactor Model and Parameters Considered (+) or Neglected (−)**			
3 m	**6 m**	**12 m**			**Model**	$\Delta \dot{n}_{total}$	p_{bed}	**Inhibition by H_2O**
30.8%	57.7%	92.0%	18.4 bar (63%)	0.24 m/s	M3	+	+	−
29.5%	53.1%	81.4%	14.3 bar [a] (49%)	0.27 m/s	M4	+	+	+

[a] The intrinsic rate (Equation (4)) at z = 12 m is 73% lower (M4) compared to no inhibition by steam (M3), and the effective rate declines by 52%, see Figures S6 and S7. Δp_{bed} is, in both cases, low (0.9 bar).

3.4. Impact of Gas Velocity on Modeling an FT Reactor if Pressure Drops, Change in Total Molar Flow Rate, and Inhibition of Reaction Rate by Steam Are Correctly Considered

Finally, the initial gas velocity $u_{s,z=0}$ was varied for the "best" model M4 and the activity C_a was 3 (Figures 8–10, Table 8). As already outlined at the end of Section 2.2, the degree and direction (decline or increase) of the change in gas velocity u_s strongly depends on the initial velocity.

If Δp_{bed} is less than 3 bar ($u_{s,z=0} \leq 0.75$ m/s), u_s decreases along the tubes by the decreasing total molar flow rate (Figure 8), and the residence time rises compared to a constant u_s by the dominating effect of the drop in the total molar flow rate; this, in return, increases $X_{CO,per\ pass}$, i.e., the "true" value (model M4) is higher compared to M1 neglecting $\Delta \dot{n}_{total}$ and Δp_{bed} (Figure 10).

For Δp_{bed} > 9 bar ($u_{s,z=0} \geq 1.25$ m/s), the effect is reverse; then, u_s increases in axial direction, the residence time decreases compared to a constant u_s, and $X_{CO,per\ pass}$ ("correct" value according to model 4) is lower compared to model 1, oversimplifying an assumed constant u_s in axial direction.

For a moderate value of Δp_{bed} of around 6 bar ($u_{s,z=0}$ = 1 m/s), the gas velocity almost remains constant in axial direction (Figure 8), i.e., the influence of $\Delta \dot{n}_{total}$ and Δp_{bed} on u_s cancel each other out (see Figure 5). For this specific case, a model with or without considering these two aspects coincidentally leads to similar results of $X_{CO,per\ pass}$ and production rate of C_{2+}-HCs (Figure 10). It should be also noted that, for this superficial gas velocity, the maximum of the rate of production of C_{2+}-HCs is reached (Figure 10, Table 8), which is contrary to the too simple model M1.

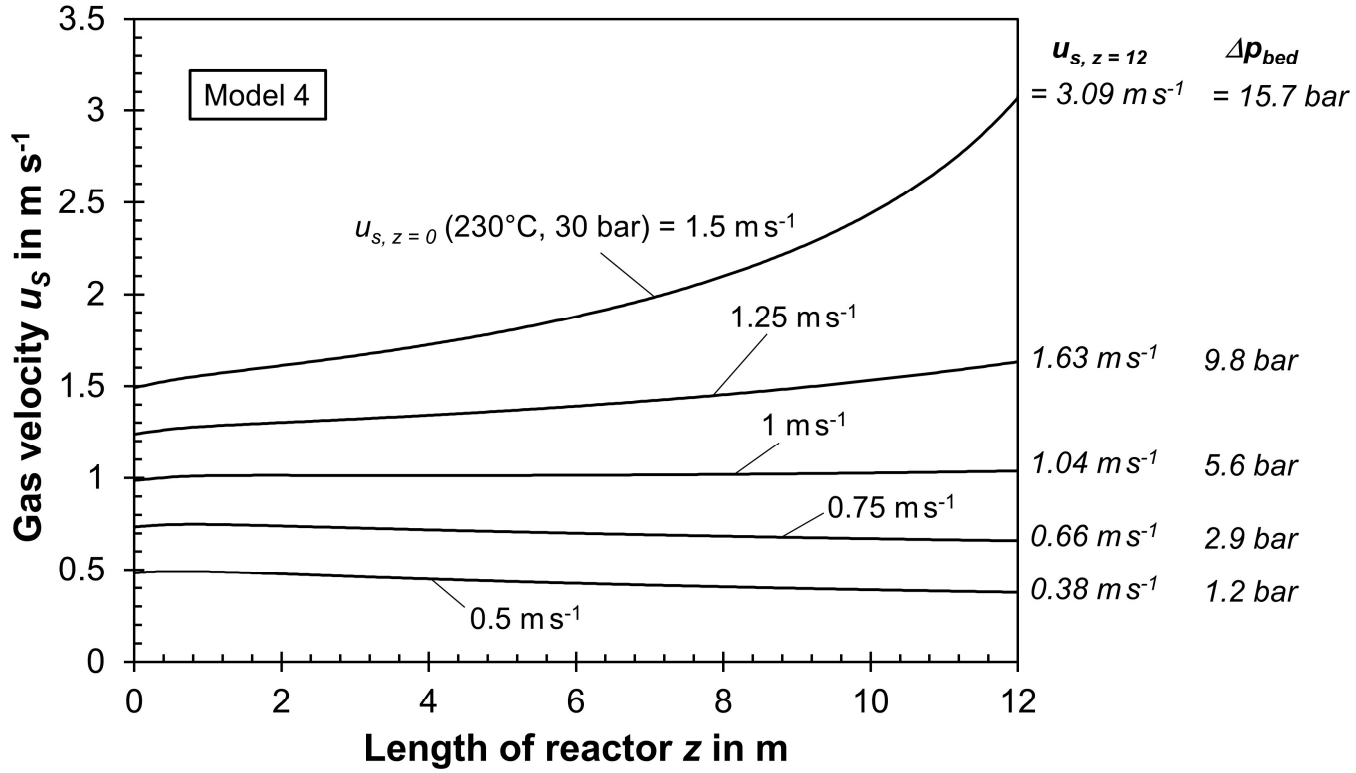

Figure 8. Influence of initial superficial gas velocity $u_{s,z=0}$ (230 °C, 30 bar) on axial profiles of u_s for the "best" model M4 (considering Δp_{bed}, change in total molar flow rate by FT reaction, and inhibition by steam/water). Reaction conditions are listed in Table 8.

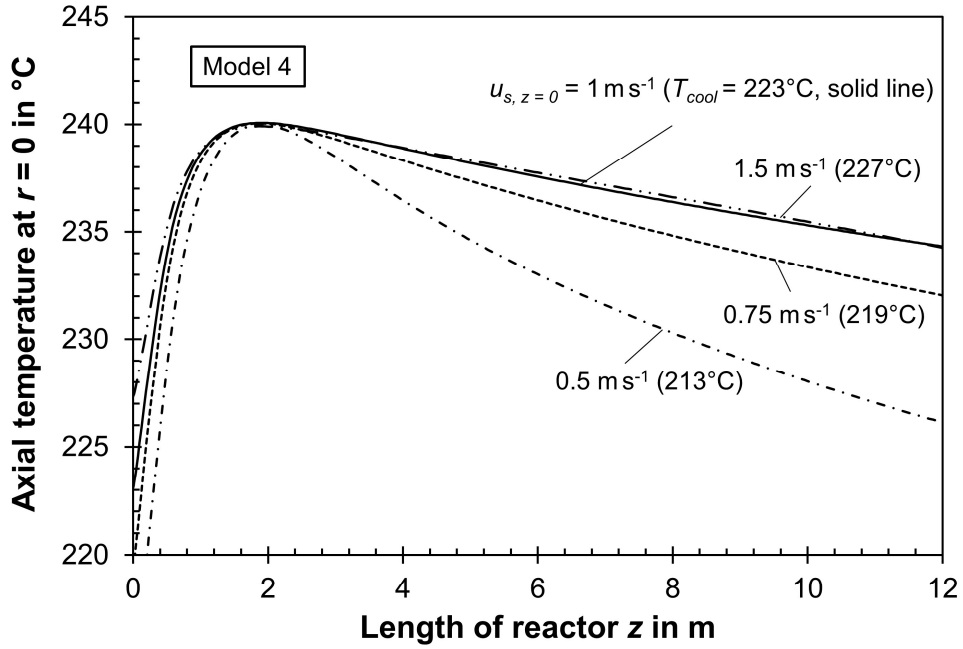

Figure 9. Axial temperature profiles for the "best" model M4 (considering Δp_{bed}, change in total molar flow rate by FT reaction, and inhibition by steam/water) for $u_{s,z=0}$ (230 °C, 30 bar) in a range of 0.5 to 1.5 m/s. Further reaction conditions are listed in Table 8.

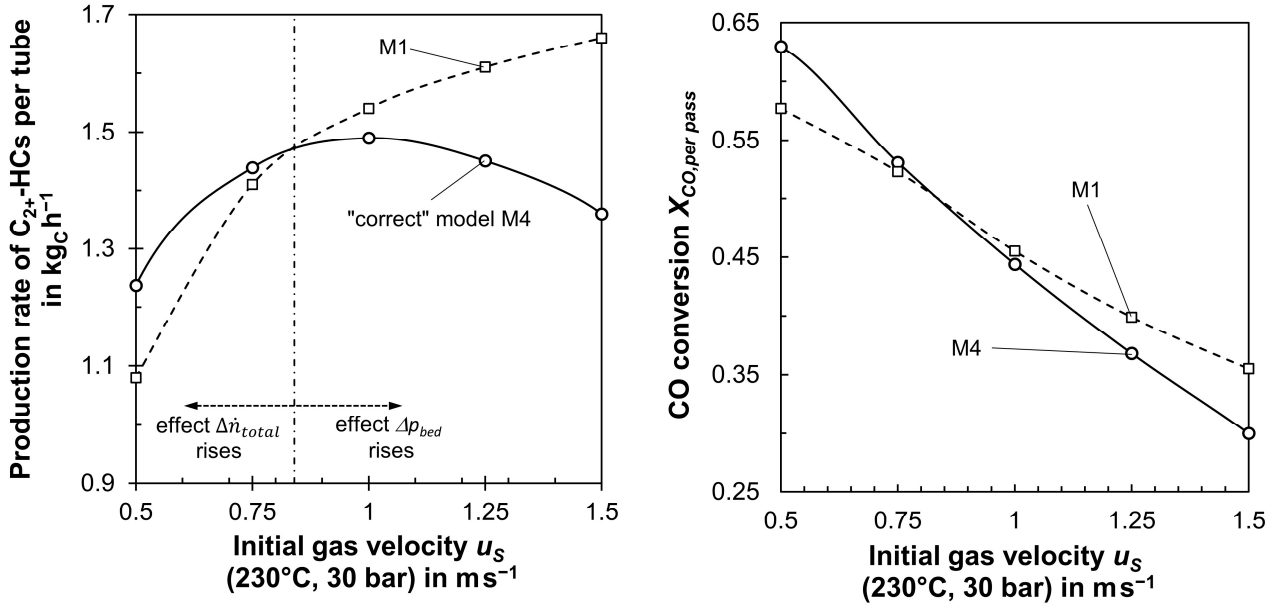

Figure 10. Influence of initial gas velocity u_s (230 °C, 30 bar) on production of C_{2+}-HCs per tube and hour of a multi-tubular reactor (**left**) and on CO conversion per pass (**right**) for the "best" model M4 (considering Δp_{bed}, change in total molar flow rate by FT reaction, and inhibition by steam/water) and for the "simple" model M1 (without considering these three factors). (C_a = 3; other reaction conditions and data are listed in Table 8.)

Table 8. Results of "best" reactor model M4: impact of initial gas velocity $u_{s,z=0}$ on the performance of a multi-tubular fixed-bed FT reactor for an axial activity C_a of 3 ($X_{CO,total}$ = 95%; S_{CH4} = 20%; molar H_2-to-CO ratio = 2.2; T_{max} = 240 °C). The axial profiles of η_{pore} (r = 0) for u_s (230 °C, 30 bar) of 0.5 and 1 m/s are shown in Figure S19.

u_s, in m/s		p_{bed}	T_{cool}	p_{cool}	$X_{CO,per\ pass}$	$y_{CH4,reactor,in}$	R	C_{2+}-HCs/Tube
z = 0 [a]	z = 12 m	in bar	in °C	in bar	in %	in %		in kg_C per h
0.23	0.17	0.3	199.6 [b]	15.2	66.1	26.5	1.04	0.64
0.48	0.38	1.2	213.3 [c]	20.1	63.2	28.4	1.10	1.24
0.73	0.66	2.9	219.4	22.9	53.1	34.0	1.73	1.44
0.99	1.04	5.6	223.1	24.6	44.4	38.7	2.49	1.49 (best case)
1.24	1.63	9.8	225.5	25.7	36.8	42.4	3.46	1.45
1.49	3.09	16.7	227.4	26.6	30.0	44.8	4.74	1.36
1.59	5.19	21.5 [d]	228.0	26.9	26.4	46.8	5.69	1.23
For comparison and illustration: Hypothetic cases for absence of mass transfer resistance by pore diffusion (η_{pore} = 1)								
0.46	0.44	1.4	191 [e]	12.9	28.9	45.8	5.01	0.43
0.94	1.07	5.7	198 [f]	14.9	28.4	46.0	5.13	0.84

[a] The values of $u_{s,z=0}$ for simulation are 0.25, 0.5, 0.75, 1, 1.25, 1.5, and 1.6 m/s and are related to 230 °C and 30 bar; the listed values at the reactor entrance are slightly lower, as $T_{cool} = T_{in}$ < 230 °C. [b] In this case, the maximum temperature of 240 °C cannot be realized (runaway): the ignition temperature (T_{ig}) is 204.6 °C and, for T_{cool} = 199.6 °C (5 K below T_{ig}), T_{max} is only 226 °C. [c] In this case, the maximum of 240 °C can just be realized without risk of thermal runaway; the ignition temperature (T_{ig}) is 220 °C and, thus, $T_{cool,max}$ is 215 °C. [d] Δp_{bed} and $u_{s,z=12m}$ increase strongly for $u_{s,z=0}$ > 1.6 m/s, see also Figure S15, e.g., for $u_{s,z=0}$ = 1.65 m/s (230 °C, 30 bar), we obtain $u_{s,z=12m}$ = 10.2 m/s (!) and Δp_{bed} = 25.5 bar (p_{final} = 4.5.bar). For such low total pressures, the kinetics were not evaluated and the model is not really reliable anymore. [e] T_{max} of 240 °C cannot be realized, T_{ig} is 196 °C, and, for $T_{cool,max}$ = 191 °C, T_{max} is only 199 °C. [f] T_{max} of 240 °C cannot be realized, T_{ig} is 203 °C, and $T_{cool,max}$ = 198 °C, and T_{max} = 208 °C. If C_a is decreased, e.g., to a value of two, T_{ig}, $T_{cool,max}$, and T_{max} are higher at 208 °C, 203 °C, and 212 °C, respectively, but, nevertheless, the CO conversion per pass is even lower (27.4%).

For completeness, it should be mentioned here that the effectiveness factor (pore diffusion) is below 0.7 for all cases listed in Table 8 (except the last two rows, where any influence of pore diffusion is deliberately neglected), even at the inlet of the fixed bed with the initially low temperature of T_{cool}, and always around 0.2 at $z \approx 2$ m, where the maximum of 240 °C is reached (Figure 9). Hence, the influence of internal mass transfer on the effective reaction rate is always strong for the given conditions, a well-known phenomenon for FT fixed-bed synthesis. For example, in the best case with regard to production of C_{2+}-HCs ($u_{s,z=0}$ = 1 m/s), η_{pore} (r = 0) is initially 0.34 at the entrance of the tubes (223 °C), drops to a minimum of 0.18 at z = 2 m, where T_{max} (240 °C) is reached, and then only slightly increases towards the end of the tubes to a value of 0.20 at z = 12 m (234 °C).

It is interesting that, in the purely hypothetic but technically not at all realistic case of the absence of any pore diffusion limitations in FT synthesis, i.e., if η_{pore} = 1 is used for the reactor simulation, $X_{CO,per\ pass}$ and, thus, also the production of C_{2+}-HCs per tube would unexpectedly even strongly decrease, e.g., for $u_{s,z=0}$ = 1 m/s from 1.49 to 0.84 kg_C h^{-1} (last row in Table 8). The allowable value of T_{cool} with regard to thermal runaway of the reactor is then only 198 °C, the maximum temperature only 208 °C, and $X_{CO,per\ pass}$ drops to 28% compared to 44% in the case correctly considering pore diffusion. For $u_{s,z=0}$ = 0.5 m/s, this effect is more pronounced and the output of C_{2+}-HCs per tube drops to 0.43 kg_C h^{-1} compared to 1.24 kg_C h^{-1} if pore diffusion is (correctly) included in the reactor simulation; see second to last row in Table 8.

The reason for this on first sight really surprising effect is the much higher reactor sensitivity if pore diffusion would not dampen the effective rate and the apparent activation energy (by a factor of about two). The thermal reactor stability without pore diffusion limitation is then only reached at a much lower cooling and maximum temperature; see Table 8 (last two rows). In other words, for FT synthesis, pore diffusion unexpectedly not only "helps" with regard to thermal stability of a multi-tubular reactor but also with regard to reaching a high CO conversion and production of HCs. This important aspect is often disregarded in evaluations of FT fixed-bed synthesis.

Additional instructive figures and a table are given in the Supporting Information:

- Figure S8 depicts the impact of $u_{s,z=0}$ on the axial profile of the total pressure in the tubes.
- Figure S9 shows the influence of u_s on the rate of heat removal from fixed bed to boiling water.
- The influence of u_s on the heat transfer coefficient $\alpha_{w,ex}$ is shown in Figure S10.
- Figure S11 shows the influence of $u_{s,z=0}$ on the axial profile of $\alpha_{w,int}$, and Figure S12 the corresponding figure for λ_{rad} in the bed of the tubes.
- Figure S13 depicts temperature profiles at different radial positions, and Figure S14 presents a selected radial temperature profile for z = 2 m (location of maximum in temperature).
- Figure S15 depicts the influence of $u_{s,z=0}$ on pressure drop and final gas velocity $u_{s,z=12m}$, indicating a strong rise both in Δp_{bed} and $u_{s,z=12m}$ with increasing $u_{s,z=0}$.
- Axial profiles of the radial heat fluxes in the tubes (heat removal, heat production, and heat flux from/to gas) are given by Figure S16.
- The parametric sensitivity of the FT reactor with and without influence of pore diffusion is also discussed in the Supporting Information (Figures S17 and S18), which explains in detail that pore diffusion "helps" with regard to thermal stability of a fixed-bed FT reactor.
- Table S1 compares an FT reactor with constant activity (C_a = 3; simulation by "optimal" model M4) with a two-zone reactor (C_a = 2.5 for z < 6 m and 3.5 for 6 m < z < 12 m) and a reactor with optimal activity distribution ($C_{a,mean}$ = 3). The data indicate that the output of C_{2+}-HCs can be improved by 4% and 8%, respectively.
- Axial profiles of η_{pore} (r = 0) for u_s (230 °C, 30 bar) of 0.5 and 1 m/s are shown in Figure S19; selected values at different temperatures are listed in Table S2.

4. Summary

In this work, a cooled multi-tubular FT reactor with a common gas recycle and purge gas stream was simulated by reactor models of different complexity, e.g., with regard to neglect or considering the pressure drop, the change in total molar flow along the tubes, or axial changes in radial heat transfer parameters. The effective reaction kinetics of CO conversion for cobalt as a catalyst were utilized in all reactor models.

An accurate and thus recommendable FT fixed-bed reactor model should consider both the change (decline for FT) in the total molar flow by the reaction and the (general) decrease in total pressure in a fixed-bed reactor by the unavoidable pressure drop. Both effects opposingly change the superficial gas velocity u_s and thus the residence time and syngas conversion, respectively, along the tubes compared to a (too) simple isobaric and isochoric (neglect of change in number of moles during reaction) reactor model presuming constant u_s. Only in rare cases do both effects cancel each other out, such as here coincidentally for u_s of 1 m/s.

A changing gas velocity as well as a drop in the total pressure along the tubes also have an impact on the radial heat transfer, i.e., on the effective thermal conductivity λ_{rad} and the heat transfer coefficient $\alpha_{w,int}$ at the internal side of the tube. Hence, these aspects should also be considered for an accurate FT reactor model.

The inhibition of the effective reaction rate by steam should be at least taken into account if a partial pressure of steam at the end of the tubes reaches more than around 5 bar. For typical reaction conditions and a common gas recycle, only a high conversion of CO of more than 50% per pass leads to such a high value of p_{H2O} at the reactor outlet.

Supplementary Materials: The following supporting information can be downloaded at: https://www.mdpi.com/article/10.3390/pr11123281/s1. Figure S1: Influence of superficial gas velocity on the heat transfer parameters λ_{rad} and $\alpha_{w,int}$; Figure S2: Axial profile of Reynolds number in the tubes of a multi-tubular FT reactor and values of λ_{rad}, $\alpha_{w,int}$, u_s, p_{total}, and v_g for two selected values of Re_p; Figure S3: Profiles of thermal resistance of tube wall and external heat transfer to boiling water and individual contributions of wall and external heat transfer alone as calculated by all models except M0; Figure S4: Profiles of reaction rate in the center of a tube of a multi-tubular FT reactor for model 3; Figure S5: Profiles of reaction rate in the center of a tube of a multi-tubular FT reactor for the model 3; Figure S6: Profiles of reaction rate of CO conversion at center of tube and CO conversion in an isothermal FT reactor for model M3 and model M4; Figure S7: Influence of CO conversion on the effective reaction rate at center of tube and steam content in an isothermal FT reactor for model M3 and model M4; Figure S8: Influence of initial superficial gas velocity on axial profile of total pressure in the tubes of a multi-tubular FT reactor; Figure S9: Influence of initial superficial gas velocity on axial profile of rate of heat removal from fixed bed to boiling water in the tubes of a cooled multi-tubular FT reactor; Figure S10: Influence of initial superficial gas velocity on axial profile of heat transfer coefficient from tube to boiling water in the tubes of a cooled multi-tubular FT reactor; Figure S11: Influence of initial superficial gas velocity on axial profile of heat transfer coefficient from fixed bed to internal tube wall in the tubes of a cooled multi-tubular FT reactor; Figure S12: Influence of initial superficial gas velocity on axial profile of effective radial thermal conductivity in the fixed bed of the tubes of a cooled multi-tubular FT reactor; Figure S13: Axial temperature profiles at different radial positions; Figure S14: Radial T-profile at the position of the axial temperature maximum; Figure S15: Influence of initial superficial gas velocity on the pressure drop and final gas velocity in the tubes of a cooled multi-tubular FT reactor; Figure S16: Axial profiles of heat fluxes in the tubes; Figure S17: Arrhenius plot of intrinsic and effective reaction rate of CO conversion at the reactor entrance; Figure S18: Influence of T_{cool} on $T_{max,ax}$ at r = 0 and on difference between $T_{max,ax}$ and T_{cool} if pore diffusion is present and for hypothetic case of absence of pore diffusion limitations; Figure S19: Axial profiles of pore effectiveness factor for a superficial gas velocity of 0.5 and 1 m/s; Table S1: Comparison of different axial distributions of the catalytic activity; Table S2: Values of pore effectiveness factor at different temperatures. References [15,16] are cited in the supplementary materials.

Author Contributions: Conceptualization, A.J.; methodology/validation, A.J. and C.K.; software/modeling, C.K.; writing, review, and editing, A.J. and C.K. All authors have read and agreed to the published version of the manuscript.

Funding: The authors gratefully acknowledge the support of the Open Access Publishing Fund of the University of Bayreuth.

Data Availability Statement: Data are contained in the article and Supporting Information.

Conflicts of Interest: The authors declare no conflict of interest.

Nomenclature

A	Cross-sectional area of tube ($\pi\ {r_t}^2$)	m^2
c_{CO}	Concentration of CO	mol m^{-3}
C_a	Coefficient of catalytic activity	
c_{CO}	Concentration of CO (gas phase)	mol m^{-3}
c_g	Total concentration (molar density) of gas phase	mol m^{-3}
c_p	Heat capacity of gas	J mol^{-1} K^{-1}
C_ϕ	Constant factor in Equation (6) (valid for d_p = 3 mm)	$kg^{0.5}$ $s^{0.5}m^{-1.5}$
d_p	Particle diameter	m
$d_{t,int}$	Internal tube diameter	m
$D_{eff,CO,liq}$	Effective diffusion coefficient of CO in liquid filled pore system	m^2 s^{-1}
f_{bed}	Friction factor of a packed bed of spherical particles	
H_{CO}	Henry coefficient for CO in liquid HCs	J mol^{-1}
L_t	Length of tube (fixed bed)	m
M_g	Molar mass of gas mixture	kg mol^{-1}
p_{final}	Total pressure at outlet of tubes	Pa
p_{total}	Total pressure (inlet of tubes)	Pa
p_{H2O}	Partial pressure of steam	Pa
Pr	Prandtl number (=$\nu_g\ c_g\ c_p/\lambda_g$)	
$\dot{n}_{\text{total}}$	Total molar flux of gas in the tubes	mol s^{-1}
r	Radial coordinate in fixed bed (radial distance from center of tube)	m
$r_{m,CO}$	Total intrinsic reaction rate of CO, see Equation (3)	mol_{CO} $kg_{cat}{}^{-1}$ s^{-1}
$r_{m,CO,H2}O$	Total intrinsic rate of CO, if inhibition by steam is considered	mol_{CO} $kg_{cat}{}^{-1}$ s^{-1}
$r_{m,CO,CH4}$	Intrinsic reaction rate of CO to of methane	mol_{CO} $kg_{cat}{}^{-1}$ s^{-1}
$r_{m,C2+}$	Intrinsic reaction rate of CO to C_{2+}-hydrocarbons	mol_{CO} $kg_{cat}{}^{-1}$ s^{-1}
$r_{m,CO,eff}$	Total effective reaction rate of CO	mol_{CO} $kg_{cat}{}^{-1}$ s^{-1}
$r_{m,CO,H2O,eff}$	Total effective rate of CO, if steam inhibition is considered	mol_{CO} $kg_{cat}{}^{-1}$ s^{-1}
r_t	Internal radius of tube	m
R	Gas constant (8.314) in Equation (6)	J mol^{-1} K^{-1}
R	Recycle ratio (ratio of recycle gas to fresh syngas)	
R_{bed}	Thermal resistance related to heat conduction ($\approx$0.25 $d_{t,int}/\lambda_{rad}$)	m^2 K W^{-1}
Re_p	Reynolds number related to particle diameter (=$u_s\ d_p/\nu_g$)	
$R_{overall}$	Overall thermal resistance (R_{bed} + $R_{w,int}$ + $R_{th,ex,total}$)	m^2 K W^{-1}
$R_{th,ex.total}$	Thermal resistance of wall (conduction) and boiling water	m^2 K W^{-1}
$R_{th,H2O}$	Thermal resistance of boiling water (convection)	m^2 K W^{-1}
$R_{th,wall}$	Thermal resistance of wall (conduction)	m^2 K W^{-1}
$R_{w,int}$	Thermal resistance related to heat transfer at internal wall ($1/\alpha_{w,int}$)	m^2 K W^{-1}
s_{wall}	Thickness of tube wall	m
S_{CH4}	Selectivity to methane related to carbon (in CO)	
T	Temperature of gas and catalyst (pseudo-homogeneous model)	°C, K
T_{cool}	Cooling temperature (constant along the tube)	°C, K
T_{ig}	Cooling temperature, where thermal runaway takes place	°C, K
T_{max}	Maximum axial temperature at r = 0 (center of tubes)	°C, K

$T_{mean,bed}$	Mean temperature of fixed bed in radial direction ($\approx T$ at $r = 0.7\ r_t$)	°C, K
$T_{rt,bed}$	Temperature of fixed bed directly at inner wall of tube, where a jump (related to $\alpha_{w,int}$) from $T_{rt,bed}$ to $T_{w,int}$ is assumed	°C, K
$T_{w,ex}$	Temperature at external wall of the tube	°C, K
$T_{w,int}$	Temperature at internal wall of the tube	°C, K
u_s	Superficial gas velocity (initial/final value: index $z = 0$ or $z = 12$ m)	m s^{-1}
$X_{CO,per\ pass}$	Conversion of CO per pass through a single tube	
$X_{CO,total}$	Total conversion of CO reached in the reactor including the gas recycle	
$y_{CH4,in}$	Molar content of CH_4 at reactor inlet	
$y_{CH4,recycle}$	Molar content of CH_4 in recycle and purge gas stream	
$y_{CO,in}$	Molar content of CO at reactor inlet	
$y_{H2,in}$	Molar content of H_2 at reactor inlet	
z	Axial coordinate in fixed bed	m
Greek letters		
α_{H2O}	Heat transfer coefficient (external area of tube to boiling water)	W m^{-2} s^{-1}
$\alpha_{w,ex}$	Heat transfer coefficient (tube to boiling water incl. heat transfer by conduction through wall, see Equation (S18))	W m^{-2} s^{-1}
$\alpha_{w,int}$	Heat transfer coefficient (bed to internal tube wall)	W m^{-2} s^{-1}
$\Delta_R H_i$	Enthalpy of reaction (i = reaction of CO to methane or to C_{2+}-HCs)	J $mol_{CO}{}^{-1}$
Δp_{bed}	Pressure drop of fixed bed (tube)	Pa
ε_{bed}	Porosity of fixed bed Thiele modulus (defined by Equation (6))	
η_{pore}	Pore effectiveness factor (defined by Equation (5))	
λ_g	Thermal conductivity of gas mixture	W m^{-1} K^{-1}
λ_{rad}	Effective radial thermal conductivity in fixed bed	W m^{-1} K^{-1}
λ_{wall}	Thermal conductivity of wall material (steel)	W m^{-1} K^{-1}
ν_g	Kinematic viscosity of gas (mixture)	mol m^{-3}
$\nu_{i,\ R_n}$	Stoichiometric coefficient of component i (i = CO, H_2, CH_2, CH_4, or H_2O) in reaction n (n = 1 for methane formation and 2 for formation of C_{2+}-HCs)	
ρ_{bed}	Bulk density of fixed bed	kg m^{-3}
Abbreviations		
C_{2+}	Hydrocarbons with two and more carbon atoms (all HCs without CH_4)	
FT(S)	Fischer–Tropsch (synthesis)	
HCs	Hydrocarbons	

References

1. Kern, C.; Jess, A. Performance of a multi-tubular Fischer-Tropsch reactor with two catalytic zones of different intrinsic chemical activity. *Catal. Sci. Technol.* **2023**, *13*, 516–527. [CrossRef]
2. Kern, C.; Jess, A. Improvement of a multi-tubular Fischer-Tropsch reactor with gas recycle by appropriate combination of axial activity distribution and gas velocity. *Catal. Sci. Technol.* **2023**, *13*, 2212–2222. [CrossRef]
3. Poehlmann, F. Zusammenspiel von Chemischer Reaktion und Porendiffusion bei der Kobaltkatalysierten Fischer-Tropsch-Synthese unter Einsatz von CO_2-Haltigem Synthesegas. Ph.D. Thesis, University Bayreuth, Bayreuth, Germany, 2017.
4. Dry, M.E. *FT Catalysts*; Fischer-Tropsch Technology, Studies in Surface Science and Catalysis; Steynberg, A.P., Dry, M.E., Eds.; Elsevier: Amsterdam, The Netherlands, 2004; Volume 152, pp. 533–600.
5. Bartholomew, C.H.; Farrauto, R.J. *Fundamentals of Industrial Catalytic Processes*; Chapter 6.5, Fischer-Tropsch Synthesis; Wiley Interscience: Hoboken, NJ, USA, 2006; pp. 398–464.
6. Gholami, Z.; Tisler, Z.; Rubas, V. Recent advances in Fischer-Tropsch synthesis using cobalt-based catalysts: A review on supports, promoters, and reactors. *Catal. Rev.* **2021**, *63*, 512–595. [CrossRef]
7. Fox, J.M. Fischer-Tropsch reactor selection. *Catal. Lett.* **1990**, *7*, 281–292. [CrossRef]
8. Jess, A.; Wasserscheid, P. *Chemical Technology: From Principles to Processes*, 2nd ed.; Wiley VCH: Weinheim, Germany, 2020.
9. Verein Deutscher Ingenieure (Ed.) *VDI-Waermeatlas: Berechnungsblaetter für den Waermeuebergang*, 9th ed.; Springer: Berlin/Heidelberg, Germany, 2002.
10. Schluender, E.-U.; Tsotsas, E. *Waermeuebertragung in Festbetten, Durchmischten Schuettguetern und Wirbelschichten*; Georg Thieme Verlag: Stuttgart, Germany, 1988.
11. Nilles, M. Waermeübertragung an der Wand Durchstroemter Schuettungsrohre. Ph.D. Thesis, University Karlsruhe, Karlsruhe, Germany, 1991.
12. Schluender, E.-U. *Einfuehrung in die Waermeuebertragung*; Vieweg, Braunschweig: Wiesbaden, Germany, 1986.
13. Stephan, K. Mechanismus und Modellgesetz des Waermeuebergangs bei der Blasenverdampfung. *Chem. Ing. Techn.* **1963**, *35*, 775–784. [CrossRef]

14. Stephan, K. *Waermeuebergang Beim Kondensieren und Beim Sieden*; Springer: Berlin/Heidelberg, Germany; New York, NY, USA; London, UK; Paris, France; Tokyo, Japan, 1988.
15. Ergun, S. Fluid Flow through Packed Columns. *Chem. Eng. Prog.* **1952**, *48*, 89–94.
16. Fritz, W. Grundlagen der Waermeuebertragung beim Verdampfen von Fluessigkeiten. *Chem. Ing. Tech.* **1963**, *35*, 753–764. [CrossRef]